



HAL
open science

Structural characterization of the interfacial self-assembly of chitosan with oppositely charged surfactant

Revaz Chachanidze, Kaili Xie, Hanna Massaad, Denis C.D. Roux, Marc Léonetti, Clément de Loubens

► **To cite this version:**

Revaz Chachanidze, Kaili Xie, Hanna Massaad, Denis C.D. Roux, Marc Léonetti, et al.. Structural characterization of the interfacial self-assembly of chitosan with oppositely charged surfactant. *Journal of Colloid and Interface Science*, 2022, 616, pp.911-920. <10.1016/j.jcis.2022.01.143>. <hal-03376419v2>

HAL Id: hal-03376419

<https://hal.science/hal-03376419v2>

Submitted on 2 Jun 2022

HAL is a multi-disciplinary open access archive for the deposit and dissemination of scientific research documents, whether they are published or not. The documents may come from teaching and research institutions in France or abroad, or from public or private research centers.

L'archive ouverte pluridisciplinaire **HAL**, est destinée au dépôt et à la diffusion de documents scientifiques de niveau recherche, publiés ou non, émanant des établissements d'enseignement et de recherche français ou étrangers, des laboratoires publics ou privés.

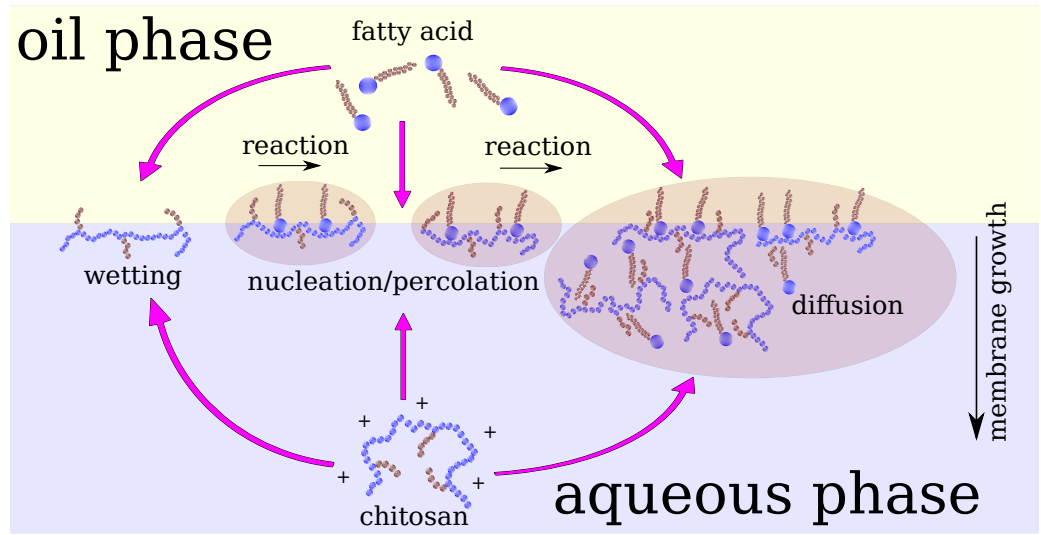


HAL Authorization

Graphical Abstract

Structural characterization of the interfacial self-assembly of chitosan with oppositely charged surfactant

Revaz Chachanidze, Kaili Xie, Hanna Massaad, Denis Roux, Marc Leonetti, Clément de Loubens



Highlights

Structural characterization of the interfacial self-assembly of chitosan with oppositely charged surfactant

Revaz Chachanidze, Kaili Xie, Hanna Massaad, Denis Roux, Marc Leonetti, Clément de Loubens

- A multiscale study of the interfacial polymerization was conducted.
- The forming interfacial membrane was probed noninvasively with a space- and time- resolved DLS approach..
- The results show spatial and temporal heterogeneities of membrane formation.

Structural characterization of the interfacial self-assembly of chitosan with oppositely charged surfactant

Revaz Chachanidze^{a,*}, Kaili Xie^{a,b}, Hanna Massaad^a, Denis Roux^a, Marc Leonetti^{a,c} and Clément de Loubens^a

^aUniv. Grenoble Alpes, CNRS, Grenoble INP, LRP, 38000 Grenoble, France

^bUniv. Bordeaux, CNRS LOMA UMR 5798, Talence F-33405, France

^cUniv. Aix-Marseille, CNRS, CINaM, Marseille, France

ARTICLE INFO

Keywords:
membrane
interface
rheology
dynamic light scattering
polyelectrolyte
biopolymer

ABSTRACT

Controlling the assembly of polyelectrolytes and surfactant at liquid-liquid interfaces offers new ways to fabricate soft materials with specific physical properties. However, little is known of the relationships between the kinetics of interfacial assembly, structural and rheological properties of such interfaces. We studied the kinetics at water-oil interface of the assembly of a positively charged biopolymer, chitosan, with an anionic fatty acid using a multi-scale approach. The growth kinetics of the membrane was followed by interfacial rheometry and space- and time-resolved dynamic light scattering. This set of techniques revealed that the interfacial complexation was a multi-step process. At short time-scale, the interface was fluid and made of heterogeneous patches. At a 'gelation' time, the surface elastic modulus and the correlation between speckles increased sharply meaning that the patches percolated. Confocal and electron microscopy confirmed this picture, and revealed that the basic brick of the membrane was sub-micrometric aggregates of chitosan / fatty acid.

1. Introduction

Since pioneering observations by Ramdsen [1] and Pickering [2] regarding the stabilization of emulsions and foams by colloidal particles trapped at interface, the interfacial assembly of colloids has seen growing interest from scientific communities. It opens the way to the fabrication of materials with specific physical properties such as films, capsules or structured liquids by using interfaces as scaffolds [3] as well as understanding some physiological functions [4]. These materials can be produced by droplet formation [5] or 3D-printing of liquid-liquid interfaces [6]. The main driving mechanism behind the self-assembly of colloids at interface is the process of minimization of interfacial energy, which can be tuned by an external stimulus [7] or by controlling the interactions between the particles [8]. As a result of this assembly, the interface can have a solid-like or liquid-like behaviour. One striking example is the possibility to design mechanically pH-responsive and self-healing microcapsules by interfacial assembly of polymer-polymer coacervates [9], which open the way to *in-situ* reconfigurable structured liquid interfaces. The rational design of self-assembled membranes with optimal properties requires an understanding of the interplay between the properties of the colloids, the kinetics of assembly and the structure of the interface.

The relation between the kinetics of interfacial assembly and the resulting physical properties such as membrane thickness or interfacial rheology has been studied for various systems, i.e. nanoparticles, polymers and polyelectrolytes. For interfaces covered by model nanoparticles [10], the structure of the interface changes with the increasing surface coverage, from a fractal network of aggregates to a heterogeneous structure with voids, to a gel with dense clusters and eventually a densely-packed system [11, 12]. Consequently, viscoelasticity and yield points of these interfaces are controlled by the surface coverage, interparticle interactions and external field forces [12, 13].

Another possible approach stabilising interfaces is via formation of an interfacial complex whereby two oppositely charged polyelectrolytes are dissolved in different immiscible phases [14, 15, 16, 17]. Upon contact, polycations and polyanions diffuse spontaneously towards the interface and form a membrane or a coacervate by electrostatic interactions. Monteillet *et al.* [15] studied the kinetics of assembly of polyelectrolytes at water-oil interfaces at macroscopic scales. They showed that the assembly was a two-stages process: a fast diffusion limited adsorption process which was followed by a much slower logarithmic process. The latter should result from the hindered interpenetration of the

*Corresponding authors: revaz.chachanidze@univ-grenoble-alpes.fr
ORCID(s): 0000-0002-4988-9168 (Clément de Loubens)

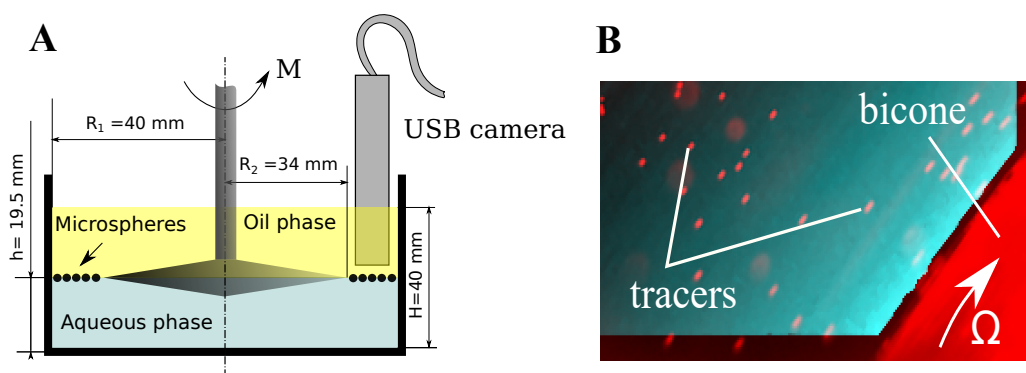


Figure 1: Interfacial rheometry by means of IRS. (A) Schematic representation of the bicone rheological cell used to probe the interfacial properties of chitosan / PFacid membrane. The interface was seeded with microparticles in order to visualize the velocity field of the interface with an immersed camera. (B) PTV at the water-oil interface, the color gradient shows the average velocity of tracers decreasing further when moving away from bicone.

26 two oppositely charged polymers, such as coacervation in the bulk. Moreover, self-consistent field analysis carried-out
 27 by the same group of authors suggested that the coacervate film should be heterogeneous [18]. H-bond acceptor and
 28 donor polymers have also been used to cover water-oil interfaces by interfacial complexation of both polymers [9]. For
 29 these systems, the elasticity is controlled by the type and strength of physical interactions [19]. Dupré de Baubigny *et*
 30 *al.* [20] investigated the kinetics of membrane growth on long time scales ($> 1,000$ s) and identified a diffusion limited
 31 process. However, the authors were surprised to observe that the process was faster when polymer molar mass incre-
 32 creased. They related this observation to the description of the structure of the membrane as a gel-like porous network,
 33 with a pore size much smaller than the radius of the diffusing polymer chains. As a result, the diffusion process should
 34 be hindered by the entropic barrier.

35 There is a growing interest in the systems formed through a complexation between polyelectrolytes and oppositely
 36 charged surfactant. Such a system has proved very useful in stabilising emulsions [21, 22], microcapsule fabrication
 37 [23, 24, 25, 26] and liposome coatings [27]. The driving force is the entropic gain due to the release of the counter-ions
 38 and water molecules [28]. In this paper, we study such process by using a model system namely complexation between
 39 a water-soluble positively charged biopolyelectrolyte, chitosan, with an oil-soluble anionic surfactant. Chitosan is
 40 highly positively charged in acidic medium due to the protonation of its amino groups (NH_3^+). The electrostatic
 41 interactions between positive NH_3^+ groups of chitosan and oppositely charged surfactants is controlled by the degree
 42 of acetylation of chitosan and pH [29, 28]. In the case of vesicles, chitosan interacts with the phospholipids bi-layer
 43 and its coverage can be strongly heterogeneous with the formation of holes [30, 31]. In the case of microcapsules, the
 44 membrane is formed by the complexation of chitosan with a fatty acid at the water-oil interface. The elasticity of the
 45 membrane increases with time and the concentration of short chain fatty acid [23, 25].

46 All these results obtained with different systems highlights the importance of structural characterization at different
 47 scales, as the interfacial coverage can be strongly heterogeneous. Moreover, given the difficulties associated with
 48 comparing the results, it is important to combine different methodologies using various interfacial characterization
 49 tools [32].

50 The aim of our work is to describe the kinetics of the assembly of a polyelectrolyte with an oppositely charged
 51 surfactant at water-oil interface using a multiscale approach. In our study, chitosan, a water soluble cationic polymer,
 52 was used to form a complex with oil-soluble anionic phosphatidic acids at water-oil interface. This system has been
 53 used for microcapsule production [23, 25, 26]. The interest of the model system for the present study, lies in the fact that
 54 its kinetics is relatively slow to study the different stages of the assembly. We characterized the kinetics of assembly at
 55 macroscopic scales by interfacial rheometer to follow the "gelation" of the interface with measurement of the velocity
 56 field of the interface. At nanometric scales, we developed space- and time- resolved dynamic light scattering (DLS) to
 57 characterize the changes in the heterogeneities of the interfaces, which was complemented by confocal and scanning
 58 electron microscopies (CSM and SEM). Lastly, this approach allowed us to relate the structure of the forming film
 59 with its rheological properties. We discuss also the analogies between this system of polyelectrolyte / surfactant with
 60 others stabilized interfaces systems.

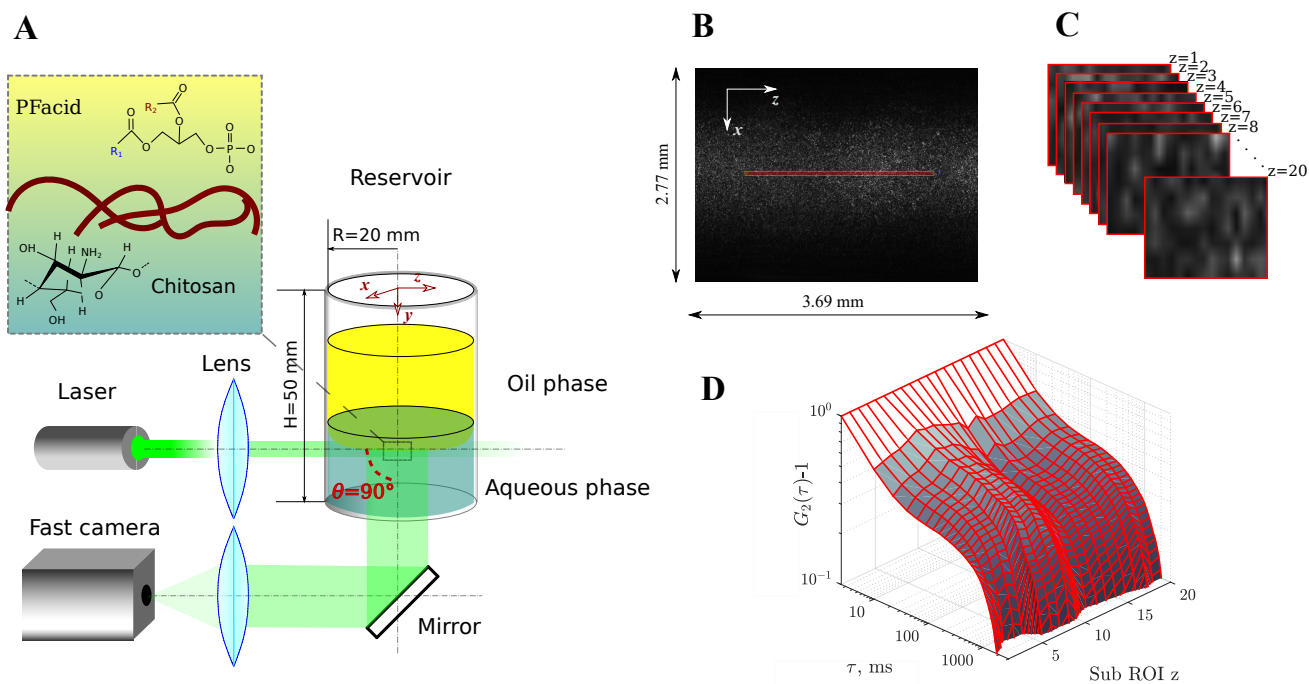


Figure 2: Representative sketch of multi-speckles Dynamic Light Scattering. (A) Chitosan / PFacid membrane was formed at oil-water interface in a cylindrical container. The interface was illuminated by a laser beam set to propagate inside the membrane. The light scattered at 90° was reflected by a polarization holding mirror and collected with a lens onto the camera sensor. (B) Example of an image taken by the CCD camera. In the center, the laser illumination path is clearly visible, showing the speckles. The red rectangle in the middle shows the part of the image used for auto-correlation calculus. (C) Stack representation of the 20th sub-ROI obtained by sequencing the red rectangle in B in equisized small images. (D) Intensity correlation function $g_2 - 1$ as a function of the lag time τ and the sub-ROI z .

61 2. Materials and methods

62 2.1. Materials

63 Chitosan (CH) powder with medium molecular weight and 75-85% deacetylation was purchased from Sigma-
 64 Aldrich ($M_w = 190\text{--}310$ kg/mol, CAS number 9012-76-4, Sigma-Aldrich). The anionic surfactant used to form a
 65 complex with chitosan at water-oil interface was phosphatidic fatty acid (PFacid). It was comprised of a commercially
 66 available lecithin known as lecithin YN (Palsgaard 4448, food-grade, E442, Palsgaard). In mass, the phosphatidic
 67 acids were 55% w/w, neutral triglycerides 40% and ammonium salts 5%. More than 90% of the fatty acid chains are
 68 C18, see [23] for details. The molecular structures of both compounds are given in Figure 2-A. Sodium hydroxide (1
 69 mol/L) was purchased from VWR. The oil-soluble fluorescent dye, Hostasol Yellow 3G (HY-3G), was acquired from
 70 Clariant. Rapeseed oil (from *Brassica rapa*, CAS number 8002-13-9), hydrochloric acid (36.5-38.0 %, BioReagent, for
 71 molecular biology) and cyclohexane (anhydrous, 99.5%, CAS number 110-82-7) were obtained from Sigma-Aldrich.
 72 Deionized water (resistivity > 18 M Ω .cm) was produced from a Millipore Filter water system. CellMask™ Deep
 73 Red Plasma membrane stain was obtained from ThermoFisher. All chemicals and solvents used in this study were
 74 commercially available and used as received unless stated otherwise.

75 The aqueous solution was obtained by dissolving chitosan powder in Millipore water and carefully adjusting the
 76 pH with hydrochloric acid (1 mol/L) at 3.0 to obtain a solution of 0.1 % w/w. The chitosan solution was then filtered
 77 to remove undissolved particles through Minisart® Surfactant-free Cellulose Acetate (SFCA) syringe Filter (pore size
 78 $5.0 \mu\text{m}$). The viscosity of the 0.1 % chitosan solution was 8 mPa·s. At pH=3.0, we can consider that all the amino
 79 groups are protonated, which corresponds to $\approx 10^3$ positive charges for one mole of the medium molecular weight
 80 chitosan used in this study [33].

81 The 1 % w/w stock solution of PFacid was obtained by dissolving lecithin YN overnight in rapeseed oil (carefully
 82 stirred at 35°C). Undissolved particles were removed by centrifugation at 1000 g for one hour. The solution was
 83 then diluted with rapeseed oil to obtain a concentration of PFacid ranging from 0.1 to 1 % w/w. The viscosity of these

84 solutions was 62.6 mPa·s at $23 \pm 1^\circ\text{C}$. If not stated otherwise, we used 0.1 % w/w chitosan solution and 0.1 % w/w
 85 PFAcid solution in order to catch assembly phenomena at short time scales. We estimated that this 1:1 ratio of mass
 86 corresponds approximately to a 1:1 ratio of free charges.

87 2.2. Interfacial rheometry

88 An interfacial rheological study of a flat film of chitosan / PFAcid complex was performed with a bicone geometry
 89 using a commercially available solution (**Figure 1**), which is an appropriate approach for interfaces with high moduli
 90 and viscosities [34]. The Interfacial Rheology System (IRS , Anton Paar, Austria) was mounted on the Modular
 91 Compact Rheometer MCR 501 (Anton Paar, Austria) after being thoroughly washed with ethanol and Milli-Q water.
 92 For the interfacial measurements, the bicone geometry was positioned at the height $H_1 = 19.5$ cm from the bottom of
 93 the measuring cell after the zero-gap was established. Then the cell was filled with the aqueous phase until the normal
 94 force acting on the geometry was not adjusted to zero point in order to position the edge of the bicone geometry exactly
 95 at the interface. Next, the oil phase was gently added over the aqueous phase up to the total height $H = 40$ cm. Every
 96 measurement was performed in 3-4 minutes after two phases were brought into contact. All oscillatory measurements
 97 were performed for at least five time periods per data point. All the measurements were conducted at room temperature
 98 ($23 \pm 1^\circ\text{C}$).

99 The interfacial viscoelastic properties of the chitosan / PFAcid membrane in oscillatory motion are described by
 100 the frequency-dependant complex linear viscoelastic modulus G_i^* ,

$$G_i^*(\omega) = G_i'(\omega) + iG_i''(\omega) \quad (1)$$

101 where G_i' and G_i'' are the components of the interfacial complex modulus (two-dimensional elastic modulus and
 102 loss modulus, respectively). It is related to the the complex interfacial viscosity η_i^* as [34]

$$G_i^*(\omega) = i\omega\eta_i^*(\omega) = -\omega\eta_i''(\omega) + i\omega\eta_i'(\omega) \quad (2)$$

103 where $\eta_i''(\omega)$ is the out-of-phase shear viscosity and $\eta_i'(\omega)$ is the the dynamic interfacial shear viscosity. The
 104 contributions of the interfacial and bulk components to the torque appearing on the bicone geometry during its motion
 105 were compared through the non-dimensional parameter, the Boussinesq number (Bo)

$$Bo(\omega) = \frac{\eta_i'(\omega) - i\eta_i''(\omega)}{a(\eta_b^{(1)} + \eta_b^{(2)})} \quad (3)$$

106 where η_b is the bulk viscosity (superscripts denote upper and lower fluid respectively) and a is the characteristic
 107 length scale that depends on the measuring system. As usual, the interfacial flow was considered to be decoupled from
 108 the bulk. In that case, the interfacial shear viscosity is calculated by [35]:

$$\eta = \frac{M - \frac{8}{3}R_2^3(\eta_b^{(1)} + \eta_b^{(2)})\Omega}{4\pi R_2^2\Omega} \quad (4)$$

109 where Ω is the angular velocity (Figure 1 A). This expression is only relevant for the $Bo \rightarrow \infty$. For low and
 110 intermediate Bo a complete analysis must be used, since the influence of the bulk phases becomes important [35].
 111 In our experiments the interfacial response was decoupled from the bulk one by using the Anton Paar application
 112 software.

113 2.3. Particle tracking velocimetry

114 The displacements and velocity field on the oil-water interface during rheometric experiments were quantified
 115 through particle tracking velocimetry (PTV). For this purpose, the water-oil interface was decorated at low coverage
 116 with polyethylene microspheres (63-75 μm Cospheric LLC, USA) used as tracers. Less than 0.01% w/w of particle
 117 powder was added to 100 mL of oil phase and mixed thoroughly with a magnetic stirrer overnight. This volume of

118 oil containing tracers was further used for rheological experiments as described above in the Section 2.2. The USB
 119 microscope (A1 USB Digital Microscope, Andonstar) was immersed in the oil phase during rheological experiments
 120 in IRS in order to visualize the displacement of microspheres under the shear flow. The image sequences were recorded
 121 at 20 frames per second and post-processed with a custom written particle tracking routine (MATLAB, MathWorks).

122 2.4. Dynamic light scattering

123 The dynamic evolution of the structure of the membrane was measured by space- and time resolved DLS at constant
 124 temperature $T=22^\circ\text{C}$. A sketch of the custom-built DLS set-up is shown in Figure 2. The oil-water interface, which later
 125 became a membrane, was illuminated by a vertically polarized laser beam produced by a single-mode laser (MSLIII,
 126 CNI, China, $\lambda = 532\text{ nm}$). The laser beam had a diameter of 2 mm and was shaped by a combination of two lenses
 127 with focal lengths $f_1 = 200\text{ mm}$ and $f_2 = -25.4\text{ mm}$. The coherent light was scattered by forming solid matter at the
 128 oil-water interface. Only the light scattered at 90° was collected, after reflection onto a non-polarized mirror. Focusing
 129 the laser beam on the interface was a complicated technical task, as the oil-water interface formed a concave-convex
 130 meniscus depending on the wettability of the cylinder. However the chitosan/PFAcid complexation leading to the
 131 membrane formation resulted in a drastic decline in interfacial tension causing the interface to flatten. This led to the
 132 interface displacement along y -axis and consequently signal loss. In order to minimise this effect, all measurements
 133 were performed using a large custom-made glass cylindrical container positioned vertically and sealed underneath with
 134 a flat sheet of glass. The dimensions of the reservoir rendered the interface displacement negligible and the precise
 135 control of the sample volume ensured the tangential contact between the interface and the laser beam throughout the
 136 experiments.

137 In order to follow the structural evolution of the membrane, the scattered intensity was collected either with a CCD
 138 camera (acA640-100gm, Basler, Germany) or with a photomultiplier (SPCM-AQR-13, excelitas Technologies, USA).
 139 When the camera was used, a lens with a focal length $f_l = 150\text{ mm}$ allowed the image of the scattering volume to
 140 form onto the CCD sensor. A diaphragm placed in the focal plane of the lens was set in order to optimize the size of
 141 the speckles to the pixel size of the camera [36]. For fast processes, the photomultiplier associated with a correlator
 142 (Flex03-LQ, Correlator.com, USA) was used to widen the dynamic range of acquisition to include lag times as small
 143 as 10^{-6} s . The wave vector q is defined as $4\pi/\lambda \sin(\theta/2)$ with λ the wavelength of the laser in the scattering medium
 144 and θ the angle of observation. As we were probing the oil-water interface, we considered the averaged optical index
 145 of both phases to calculate λ (1.333 for water and 1.471 for the oil). Consequently, the wave vector q was $23 \pm 2\ \mu\text{m}^{-1}$.

146 Our approach enabled nondestructive probing of the interfacial membrane evolution with both spacial and temporal
 147 resolution, as long as the characteristic relaxation time of the studied system allows signal detection with a digital
 148 camera. The scattered light detected by CCD camera created the image of a coherence area known as speckle (Figure
 149 2 B). The red rectangle in the center of the image represents the Region Of Interest (ROI), only this part of the image
 150 has been used for analysis. This area was sequenced into 20 sub-ROI (Figure 2 C). The laser beam passing through the
 151 interface created a trace that was visualised by CCD camera as bright area in the middle of the image along z -direction
 152 (see Figure 2 B). The region of interest was chosen in the middle of that area and was limited by 10 pixels along
 153 x -direction. This choice was justified by a compromise between the image size and the readout speed of CCD camera.
 154 The individual time autocorrelation function of the scattered intensity $g_2(\tau) - 1$ was computed for each sub-ROI

$$155 \quad g_2(\tau, z) - 1 = \frac{\langle I^z(t)I^z(t + \tau) \rangle_t}{\langle I^z(t)^2 \rangle_t} - 1 \quad (5)$$

156 where $I^z(t)$ is the intensity collected within z^{th} sub-ROI and $\langle \dots \rangle_t$ denotes averaging over time. Figure 2 D shows
 157 the result of the intensity correlation function as a function of the sub-ROI z and the lag time τ .

158 We also used the Time Resolved Correlation scheme (TRC) which allows DLS investigation of heterogeneous
 159 dynamics, as introduced by [37, 38, 39]. Analogously to $g_2(\tau) - 1$, the correlation degree $c_I(t, \tau, z)$ was calculated
 159 individually for each sub-ROI z

$$160 \quad c_I(t, \tau, z) = \frac{\langle I_p^z(t)I_p^z(t + \tau) \rangle_p}{\langle I_p^z(t) \rangle_p \langle I_p^z(t + \tau) \rangle_p} - 1 \quad (6)$$

160 where p is a pixel of the sub-ROI z , I_p^z the pixel intensity and $\langle \dots \rangle_p$ denotes averaging over pixels in the sub-ROI.

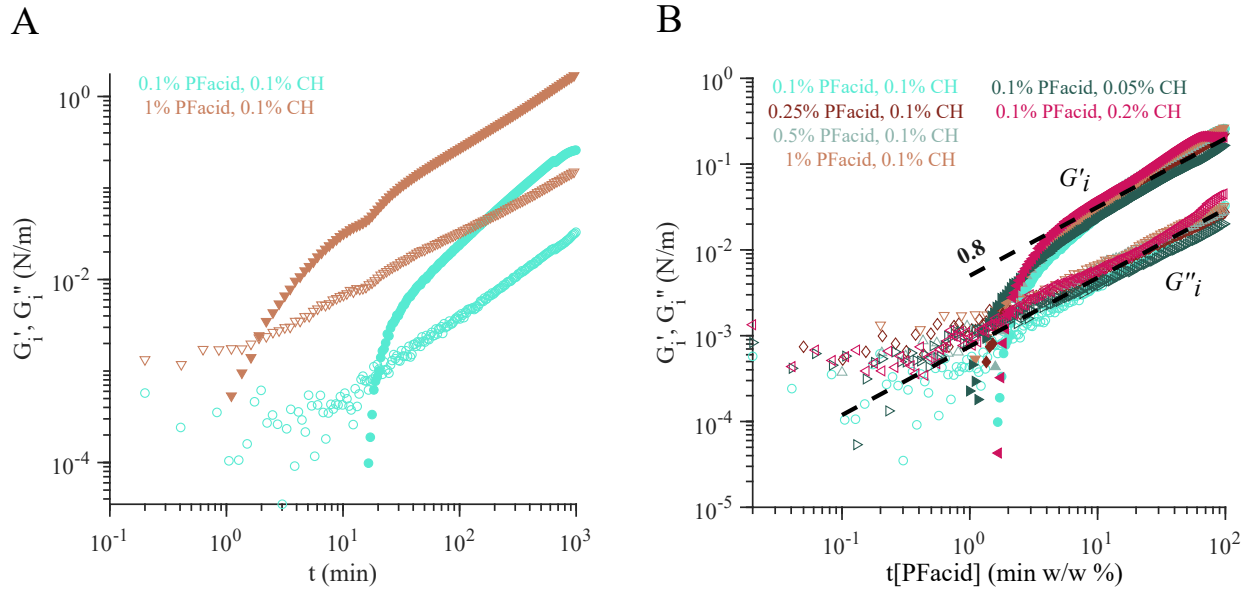


Figure 3: Macroscopic study of the interfacial rheological properties of a chitosan / PFacid membrane. (A) Typical time-dependant evolution of interfacial elastic G'_i (filled symbols) and viscous G''_i (empty symbols) shear moduli at different concentrations of PFacid. $f = 0.5$ Hz, $\dot{\gamma} = 0.03\%$, chitosan 0.1% w/w (B) The kinetics of G'_i and G''_i collapsed on the same master curves when the time axis was multiplied by the concentration of PFacid, for various concentrations of PFacid and chitosan.

2.5. Microscopy

SEM was used to characterize the morphology of chitosan / PFacid membrane. The membranes were grown on the surface of chitosan drops suspended in oil phase which contained PFacid. Once the required complexation time was achieved the droplets were washed with a large quantity of cyclohexane (for more details see [23], [25]) in order to remove the oil with the residues of anionic surfactant. The chitosan droplets encapsulated with the membrane were placed on a cover slip and dried at room temperature. Dried chitosan / PFacid membrane were observed with SEM. Samples were coated with Au/Pd in a Baltec MED-020 sputter coater and observed in secondary electron mode in a Thermo Scientific Quanta 250 microscope equipped with a field emission gun and operating at 2.5 kV.

CSM was also used to characterize the morphology of chitosan / PFacid membrane in wet conditions. Analogously to the SEM characterization described above, the chitosan droplets were injected into oil phase containing anionic surfactant. Wet (no cyclohexane washing) chitosan / PFacid membrane were observed with Leica TCS SP8 scanning point confocal microscope equipped with a $\times 63$ oil immersion objective and in-plane image resolution $0.36 \mu\text{m}/\text{px}$.

3. Results and discussion

3.1. Interfacial rheology of chitosan / PFacid membrane

We analysed the kinetics of formation of the membrane with a time sweep experiment at constant amplitude ($\dot{\gamma} = 0.03\%$) and frequency ($f = 0.5$ Hz). The choice of these parameters was justified by a compromise between signal sensibility and minimizing the disturbance of the interfacial complexation process by the stress. Moreover, this set of parameters allowed us to keep the deformation within the linear viscoelastic regime at long time scales (after 16h, see Figure SI 1). However, as explained below, the growth of the membrane was disturbed by the applied strain. Figure 3-A depicts the evolution of G'_i and G''_i over time for two different concentrations of PFacid. Note that the 1:1 mass ratio corresponds approximately to a 1:1 ratio of free charges. As a control, a pure water-oil interface without membrane formation was also quantified (see Figure SI 2), which showed a constant G''_i of $\sim 10^{-3}$ N/m whereas G'_i was null. In the early stage of membrane formation ($t < 1$ min for 1% w/w PFacid and 10 min for 0.1% w/w PFacid), G''_i was almost constant and close to the system without PFacid. G'_i was out of the measurement sensitivity. In this regime, the interface manifested purely liquid-like properties. However, within a few minutes, a slow increment in G''_i was accompanied by a rapid growth of G'_i . The interfacial storage modulus G'_i quickly overcame G''_i , manifesting the prevalence of solid-like properties. On long time scales, both interfacial moduli increased.

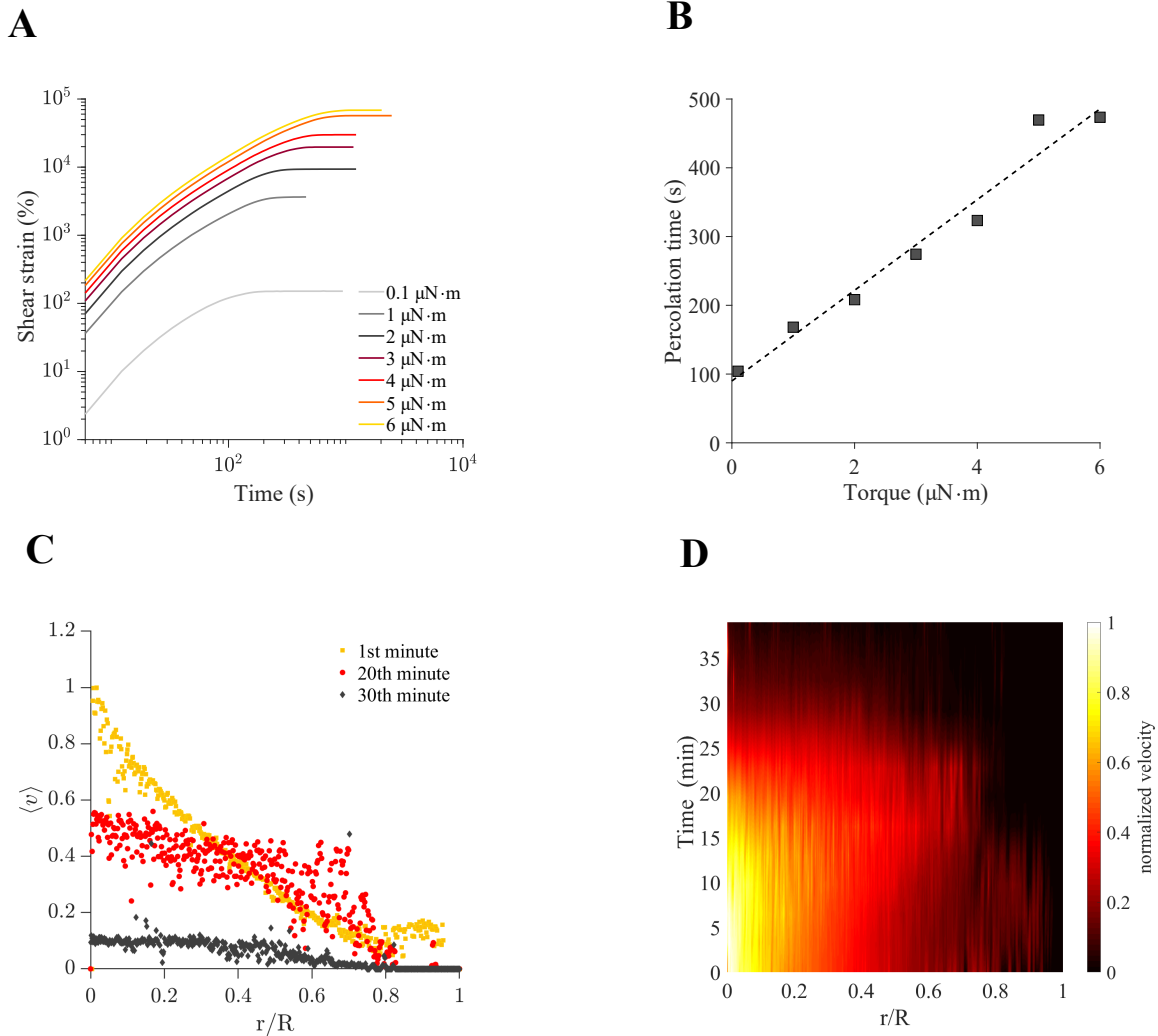


Figure 4: Particle tracking on the water-oil interface during the creep experiment. Chitosan 0.1% w/w, PFAcid 0.1% w/w.

(A) Creep experiments at the water-oil interface during the membrane formation at different torque values. (B) The time required to stop the rotation of the geometry increased on a roughly linear basis with the torque. (C) Normalized velocity profiles at the interface at different stages of membrane formation. $r/R = 0$ is the edge of the bicone. (D) The heatmap of normalized velocity values at the different points in time.

188 To gain insight into the mechanisms at play in the early moments of membrane formation, creep experiments on the
 189 forming membrane were coupled to visualisation of the deformation of the interface by PTV (Figure 4). In these creep
 190 experiments, the bicone geometry was put into motion at fixed torque values and the deformation was measured. As the
 191 membrane was forming, the shear strain increased gradually until the geometry was brought to arrest. The evolution
 192 of the deformation varied with the applied torque, Figure 4-A. In analogy with percolation of particle laden interfaces
 193 [10], we termed the time at which the strain rate was null, the percolation time. The percolation time increased on a
 194 roughly linear basis with the applied torque, Figure 4-B. Thus, the percolation process of the interface was coupled to
 195 the interfacial shear rate. We deduced from the intercept of the linear fit at zero torque, that the percolation time in
 196 absence of flow disturbance tended to 100 s.

197 The water-oil interface was decorated at low coverage with polyethylene microspheres ($\sim 70 \mu\text{m}$) used as tracing
 198 particles. The radial velocity profile v of the interface was parabolic during the first few minutes of reaction, as
 199 expected for liquid interfaces. The spatio-temporal evolution of the velocity shows that the geometry slow-down was
 200 associated with the flattening of the velocity profile, Figure 4-C,D. Macroscopically, we observed that the shear rate
 201 tended towards zero in regions closed from the geometry ($r = 0$ and R). However, the velocity distribution was strongly
 202 heterogeneous before the arrest of the geometry. In fact, a closer look at the interface showed a constant formation

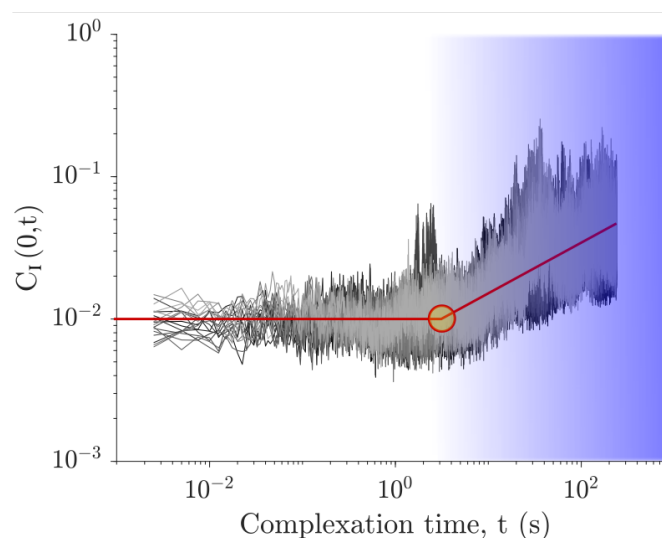


Figure 5: Time Resolved Correlation (TRC) at 0 lag time (τ) of building interface of the 20 ROIs. Straights lines and the color background are eye-guides and the circle at line interception indicates the starting time of the membrane gelation. Chitosan 0.1% w/w, PFAcid 0.1% w/w.

203 and rupture of the membrane. We observed millimetric patch-like sheet membranes that grew all over the interface
 204 and accumulated close to the geometry (see **Supporting video**). When the amount of membrane pieces was high
 205 enough to fully cover the interface, the interface jammed and stopped the motion of the geometry. This result fitted
 206 with non-reactive particle laden-interface for which domains of packed particles create elastic interfaces. When these
 207 domains start to break-up, a transition to viscous-like behavior was observed [40].

208 Then, we repeated the time sweep experiments for various concentrations of PFAcid and chitosan. We observed
 209 that the kinetics was mainly dependent on the PFAcid concentration. In Figure 3-B, we multiplied the time axis by the
 210 concentration of PFAcid. We observed a good collapse of the different curves for both interfacial moduli. We deduced
 211 from this master-curve that the percolation time increased linearly with the concentration of anionic surfactant. On
 212 long-time scales, both moduli scaled with $(t[\text{PFAcid}])^{0.8}$ (dashed lines), whereas the chitosan/PFAcid film thickness
 213 scales with the square-root of the time (see **Supporting material**). We could interpret this as a non-homogeneous
 214 growth of the membrane. We have to be cautious with the interpretation of the slope of viscoelastic moduli, as it
 215 was not possible to carry out the measurements within the linear viscoelastic regime during the course of membrane
 216 formation. However, all these features indicated that the growth of the membrane at long time scales was limited by
 217 the diffusion of the surfactant in the membrane under formation, similarly to interfacial polymer complexation [20].

218 Finally, we concluded that the complexation of chitosan with PFAcid is a two-step process. At short time scale,
 219 the interface has a macroscopic rheological behaviour which is characteristic of liquid interfaces, but the interface is
 220 strongly heterogeneous and is composed of solid patches. At a critical time, termed the percolation time, the millimetric
 221 patches pave the interface and percolate, which is characterized by a sudden increase of the interfacial elastic modulus
 222 G'_I . This process depends on both the hydrodynamic conditions and the concentration of the diffusing surfactant.
 223 These observations are also analogous to gelation of polymer under shear, for which there is a competition between
 224 the formation of clusters that tend to form a percolated network and hydrodynamic forces that disrupted the network
 225 [41]. At long time scales, the thickness of the membrane grew by diffusion of the surfactant in the membrane under
 226 formation, as observed during the interfacial complexation of polymers [20].

227 3.2. Dynamic light scattering experiments

228 In order to shed light on the structural evolution of the interface formation at a smaller length scale, we employed
 229 DLS and time-resolved correlation (TRC) analysis [37, 38, 42], see Figure 2 for the experimental set-up. The length
 230 scale that we probed with our set-up was of 40-45 nm. The interface was formed at the water-oil interface in a cylindrical
 231 reservoir via complexation between 0.1 % w/w chitosan and 0.1 % w/w PFAcid, Figure 2. During the first 2 s, $C_I(\tau = 0, t)$
 232 fluctuated randomly around a steady value of $\approx 10^{-2}$, Figure 5. Such behaviour corresponds to a Brownian system
 233 [37, 39], meaning that the displacement of particles between any two frames was on average the same, independently

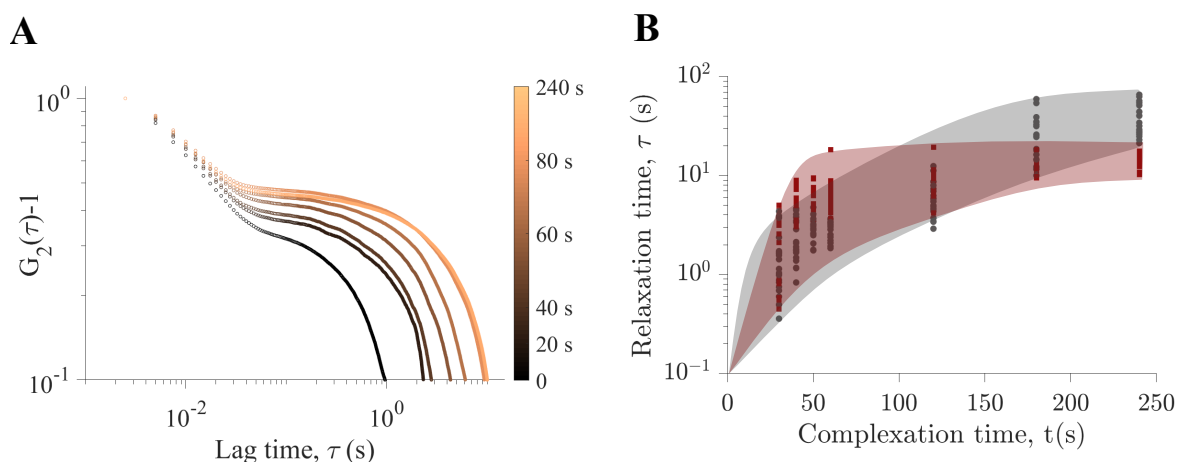


Figure 6: (A) Auto-correlation function of the interface computed from the mean time of TRC as at different lag times for an ROI as a function of the time from 0 to 240 s. (B) Evolution of the relaxation times of the forming interface within different sub-ROI computed for two separate experiments at identical conditions. The colored areas separating two experiments serve as guiding lines. Chitosan 0.1 % w/w, PFAcid 0.1 % w/w.

234 of the complexation time t . Beyond 2 s, the resolved correlation function drastically increased and gained half a decade
 235 in 100 s, meaning that the degree of correlation in the sample increased. This behaviour indicated the formation of a
 236 gel-like interface at the scale of 40-45 nm [37].

237 The kinetics of membrane formation was also probed with the intensity correlation function $G_2(\tau) - 1$. Figure 6-A
 238 shows the intensity correlation function computed at different lag times following the formation time of the membrane
 239 from 0 to 240 s. At 0 s, the intensity correlation function was identical to the correlation of the chitosan alone (see
 240 **Supporting material**) with a relaxation time of 0.1 s. As the time increased, a second relaxation time appeared as a
 241 second mono-exponential function for which relaxation time increased from 0.1 s to more than 10 s in 200 s of mem-
 242 brane complexation. After long complexation (10 hours), the characteristic relaxation time of a membrane increased
 243 up to 2×10^3 (see **Supporting material**).

244 The results of spatial analysis are depicted in Figure 6-B, where each dot corresponds to an ROI of $56 \mu\text{m} \times 56 \mu\text{m}$.
 245 Initially, the relaxation time at the interface was the same as that of the chitosan. As the chitosan / PFAcid complexation
 246 took place and a solid matter started to appear at the interface, the relaxation time increased. At the different com-
 247 plexation times considered here, the relaxation times differed by nearly one decade between different ROI. It indicated
 248 high dynamic heterogeneity in the interface complexation. This was consistent with the observation of patches dur-
 249 ing the interfacial rheological measurement. We concluded that interfacial complexation of chitosan with the anionic
 250 surfactant PFAcid is a spatially heterogeneous process.

251 3.3. Scanning electron and confocal microscopy

252 The morphology of chitosan / PFAcid membranes was observed with SEM. In order to minimise harsh manipula-
 253 tions with fragile membranes, chitosan / PFAcid membranes were grown on a surface of water droplets in oil phase
 254 containing chitosan and PFAcid respectively, for more details see [25]. The complexation reaction was stopped by a
 255 gentle washing in large quantities of cyclohexane. After that, the droplets now enclosed by a solid membrane were
 256 placed on the glass substrate and dried prior the SEM imaging.

257 Figure 7 demonstrates the morphology of the chitosan / PFAcid formed at 0.5 and 2 min. The membrane formed at
 258 0.5 min (Figure 7 A) was characterized by an important heterogeneity of its structure. It appeared to be formed out of
 259 a large number of non-connected patches of 1-5 μm . Additionally, large non-circular holes up to 10 μm were found in
 260 the membrane. Although these large perforations of the membrane could be attributed to the damage during sample
 261 preparations, the presence of non-connected patches fitted with our previous analysis. At 2 minutes of complexation
 262 the membrane appears to be intact although the presence of large circular holes can be noted on occasion (Figure 7 B),
 263 that fit with a percolated network. The circular shape of the voids could be due to the effect of surface tension. Figure
 264 7 C shows a magnification of the same membrane which was quite granular. Figure 7 D shows the transverse view of
 265 the membrane, which was characterized by sub-micrometric aggregates.

266 The confocal imaging was carried out at 1 minute complexation time in order to visualize the initial stages of

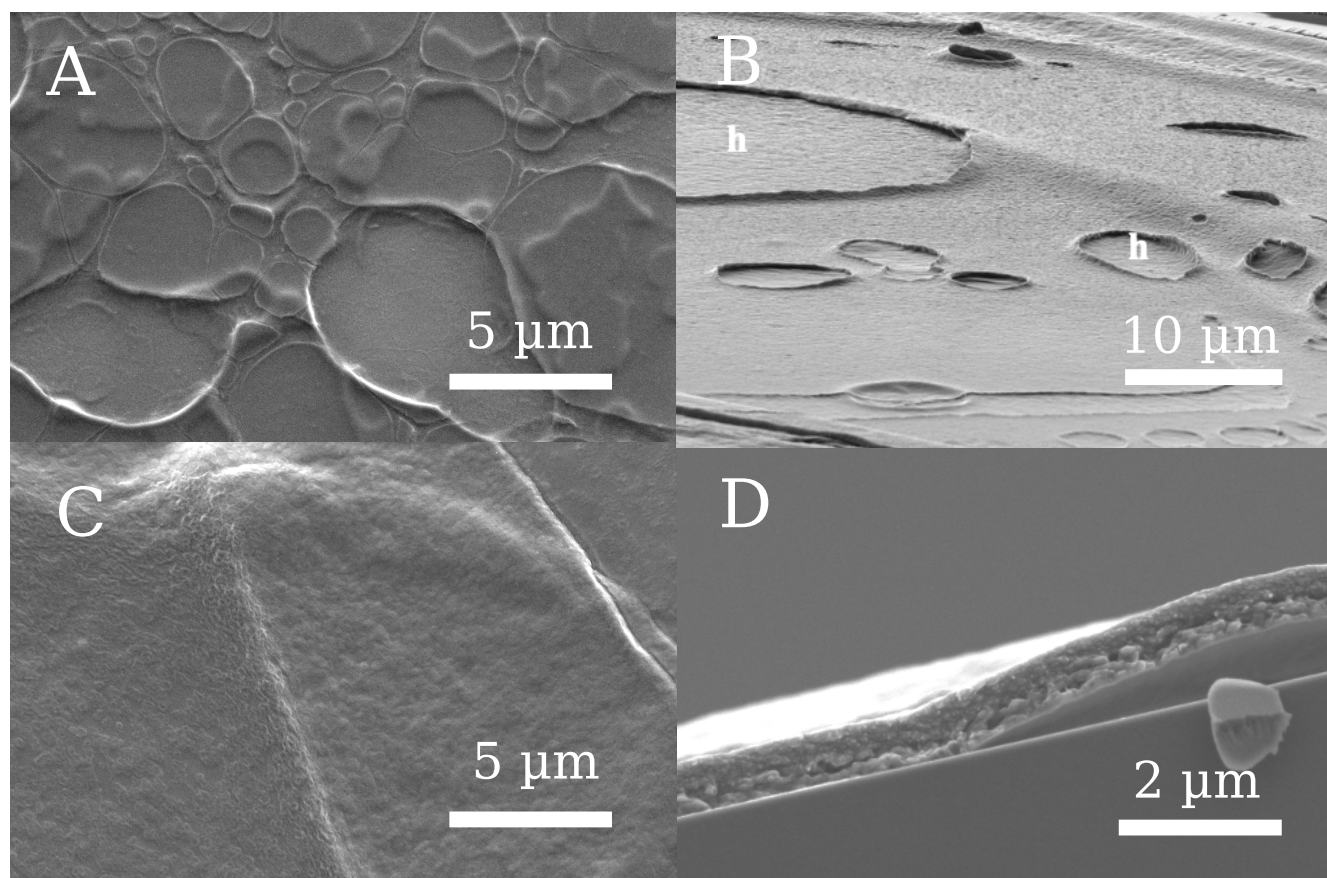


Figure 7: SEM images of dried chitosan / PFacid membrane. (A) CH / PFacid membrane after 30s of complexation. The interface was made of individual patches of 1-50 μm size (p), as well as large holes (h). (B) CH / PFacid membrane after 2 min of complexation. The interface was homogeneous, with the exception of circular holes (h). (C) CH / PFacid membrane after 2 min of complexation. The interface is fully formed though characterized by a certain roughness. (D) View in the thickness of the membrane after 2 min of complexation. The membrane showed a granular structure. Chitosan 0.1 % w/w, PFacid 0.1 % w/w.

267 membrane formation and on the thick membrane after 48h of complexation in order to reveal the internal structure of
 268 the interface. Water droplets containing 0.1 % w/w concentration of chitosan were injected into the oil phase containing
 269 0.1 % w/w concentration of PFacid. Water-soluble fluorescent dye with high lipid affinity (CellMask™ Deep Red
 270 plasma membrane stain, Invitrogen™) was added to the aqueous phase. This dye has little to no fluorescence in a free
 271 form and is only fluorescent once it is "anchored" to lipids. Figure 8 depicts the results of confocal imaging. Note
 272 that the environmental conditions of observations were very different from SEM imaging, where the membrane was
 273 dried before visualization. After 1 min of complexation, the side view of the interface shows the presence of discrete
 274 nano-metric patches, Figure 8-A. At long time scales, these inclusions formed a continuous membrane, Figure 8B-D.
 275 Figure 8-D shows the concentration gradient of these inclusions from the oil phase towards the aqueous phase. As the
 276 fluorescent dye anchored to lipids, we deduced that this gradient of light intensity corresponds to a gradient of PFacid.

277 This set of microscopy images consolidated the idea that membrane formation was due to the percolation of in-
 278 dividual patches. When the patches were able to form a percolated network, large holes were present. These results
 279 were reminiscent of interfaces covered by model nanoparticles which form heterogeneous structures with voids for
 280 low particle surface coverage [12, 11, 10]. The basic bricks are sub-micrometric aggregates of chitosan/PFacid. On
 281 long time scales, the membrane was fully covered of these aggregates. In the thickness of the membrane, there was a
 282 negative gradient of these aggregates from the oil phase to the water phase. This last result supports the idea that the
 283 growth of the membrane was limited by the diffusion through a gel-like porous network of PFacid on long time scales,
 284 as described for H-bond donor / acceptor polymers [20].

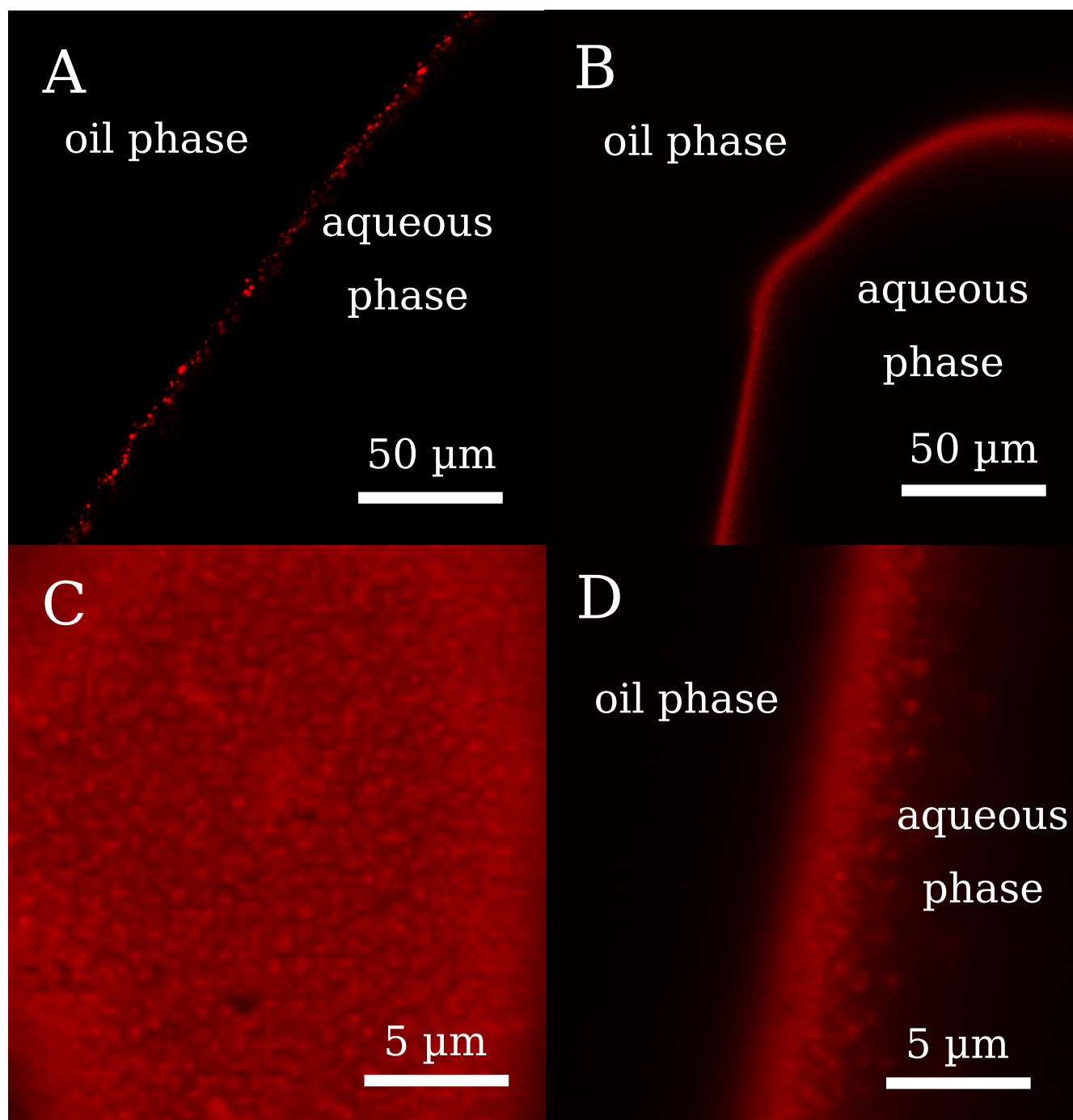


Figure 8: Confocal images of wet Chitosan / PFacid membrane, the membrane was marked by a fluorescent dye with high lipid affinity (see text for details). (A) lateral optical slice of a membrane after 1 minute of complexation. (B) lateral optical slice of a membrane after 48h of complexation. (C) A piece of a membrane laying flat on a glass substrate showing a granularly patterned structure, 48h of complexation (D) A horizontal confocal slice of a labeled membrane, 48h of complexation. Chitosan 0.1 % w/w, PFacid 0.1 % w/w.

285 4. Conclusion

286 Membrane formation based on the complexation between chitosan and short chain fatty acid has been used as a
 287 model for interfacial self-assembly of polyelectrolytes and charged surfactant. A multi-scale approach was used in
 288 order to perform a characterisation of membrane formation and morphology.

289 The multiscale approach created a robust overarching picture of the interfacial complexation process that we sum-

up here. The basic bricks of these membranes are sub-micrometric aggregates of chitosan and surfactant, that were observed by SEM and CSM (Figure 7, 8). The structure of these aggregates is an open question. At the early stage of membrane formation, the interface behaved like a fluid at macroscopic scale (Figure 1-a), and the spatial degree of correlation was low at length scales of 40-45 nm (Figure 5-a). Then, solid patches emerged and increased in size and/or number, which was visible at different length scales. At the smallest length scale used in this study, this corresponded to a sudden increased of the spatial correlation probed by DLS (Figure 5-a). At micrometric scales, individual patches were visible by SEM (Figure 7-a). At macroscopic scales, millimetric patches transported by the interfacial flow were also visible in rheometric experiments. The elastic behaviour emerged suddenly when the patches percolated (Figure 1, 4). The formation of the percolated network was also supported by SEM images that showed the presence of a continuous network with voids (Figure 7-b). The process of percolation was mainly dependent on the interfacial stress and the concentration of PFacid. On long time scales, the growth of the membrane was limited by diffusion of the surfactant.

In conclusion, the interfacial structuring of chitosan with the anionic surfactant is strongly analogous to bulk gelation of polymers [41] and shared some common features with different interfacial systems such as nanoparticles, [13, 12, 10] polymer or polyelectrolytes [9, 19, 20]. Finally, this work brings new elements on interfacial complexation that should prove useful to control the properties of liquid-liquid interfaces for the design of new materials, such as microcapsules or structured liquids.

5. Acknowledgements

LRP is part of the LabEx Tec21 (ANR-11-LABX-0030) and of the PolyNat Carnot Institute (ANR-11-CARN-007-01). The authors express their sincere gratitude to Christine Lancelon-Pin (CERMAV-CNRS, Grenoble, France) for her assistance with scanning-electron microscopy. The authors acknowledge the NanoBio-ICMG chemistry platform (UAR 2607, Grenoble) for granting access to the electron microscopy facilities. The authors thank the support of ANR 2DVisc (ANR-18-CE06-0008-01).

6. Author contributions

Revaz Chachanidze: Conceptualization, Methodology, Formal analysis, Investigation, Writing - Original Draft, Visualization **Kailie Xie:** Conceptualization, Methodology, Investigation, Writing - Review & Editing **Hanna Mas-sad:** Methodology, Formal analysis, Investigation, Writing - Original Draft, Visualization **Denis Roux:** Methodology, Formal analysis, Writing - Original Draft, Supervision **Marc Leonetti:** Conceptualization, Methodology, Writing - Original Draft, Supervision **Clément de Loubens:** Conceptualization, Methodology, Writing - Original Draft, Supervision

References

- [1] W. Ramsden, Separation of solids in the surface-layers of solutions and 'suspensions' (observations on surface-membranes, bubbles, emulsions, and mechanical coagulation).—preliminary account, Proceedings of the royal Society of London 72 (477-486) (1904) 156–164.
- [2] S. U. Pickering, Cxciv.—the interaction of metallic sulphates and caustic alkalis, Journal of the Chemical Society, Transactions 91 (1907) 1981–1988.
- [3] J. Forth, P. Y. Kim, G. Xie, X. Liu, B. A. Helms, T. P. Russell, Building reconfigurable devices using complex liquid–fluid interfaces, Advanced Materials 31 (18) (2019) 1806370.
- [4] P. Bertsch, J. Bergfreund, E. J. Windhab, P. Fischer, Physiological fluid interfaces: Functional microenvironments, drug delivery targets, and first line of defense, Acta Biomaterialia (2021).
- [5] E. Amstad, Capsules: Their past and opportunities for their future (2017).
- [6] R. Xu, T. Liu, H. Sun, B. Wang, S. Shi, T. P. Russell, Interfacial assembly and jamming of polyelectrolyte surfactants: A simple route to print liquids in low-viscosity solution, ACS Applied Materials & Interfaces 12 (15) (2020) 18116–18122.
- [7] A. Maestro, Tailoring the interfacial assembly of colloidal particles by engineering the mechanical properties of the interface, Current opinion in colloid & interface science 39 (2019) 232–250.
- [8] J. N. Israelachvili, Intermolecular and surface forces, Academic press, 2015.
- [9] J. D. de Baubigny, C. Trégouët, T. Salez, N. Pantoustier, P. Perrin, M. Reyssat, C. Monteux, One-step fabrication of pH-responsive membranes and microcapsules through interfacial h-bond polymer complexation, Scientific reports 7 (1) (2017) 1–7.
- [10] J. H. Thijssen, J. Vermant, Interfacial rheology of model particles at liquid interfaces and its relation to (bicontinuous) pickering emulsions, Journal of Physics: Condensed Matter 30 (2) (2018) 023002.
- [11] S. Reynaert, P. Moldenaers, J. Vermant, Interfacial rheology of stable and weakly aggregated two-dimensional suspensions, Physical Chemistry Chemical Physics 9 (48) (2007) 6463–6475.

- 341 [12] K. Masschaele, J. Fransaeer, J. Vermant, Direct visualization of yielding in model two-dimensional colloidal gels subjected to shear flow,
342 *Journal of rheology* 53 (6) (2009) 1437–1460.
- 343 [13] M. Cui, T. Emrick, T. P. Russell, Stabilizing liquid drops in nonequilibrium shapes by the interfacial jamming of nanoparticles, *Science*
344 342 (6157) (2013) 460–463.
- 345 [14] D. Grigoriev, T. Bukreeva, H. Möhwald, D. Shchukin, New method for fabrication of loaded micro- and nanocontainers: emulsion encapsulation
346 by polyelectrolyte layer-by-layer deposition on the liquid core, *Langmuir* 24 (3) (2008) 999–1004.
- 347 [15] H. Monteillet, F. Hagemans, J. Sprakel, Charge-driven co-assembly of polyelectrolytes across oil–water interfaces, *Soft Matter* 9 (47) (2013)
348 11270–11275.
- 349 [16] G. Kaufman, R. Boltysanskiy, S. Nejadi, A. R. Thiam, M. Loewenberg, E. R. Dufresne, C. O. Osuji, Single-step microfluidic fabrication of soft
350 monodisperse polyelectrolyte microcapsules by interfacial complexation, *Lab on a Chip* 14 (18) (2014) 3494–3497.
- 351 [17] M. Kim, S. J. Yeo, C. B. Highley, J. A. Burdick, P. J. Yoo, J. Doh, D. Lee, One-step generation of multifunctional polyelectrolyte microcapsules
352 via nanoscale interfacial complexation in emulsion (nice), *ACS nano* 9 (8) (2015) 8269–8278.
- 353 [18] H. Monteillet, J. Kleijn, J. Sprakel, F. Leermakers, Complex coacervates formed across liquid interfaces: A self-consistent field analysis,
354 *Advances in colloid and interface science* 239 (2017) 17–30.
- 355 [19] S. Le Tirilly, C. Tregouët, S. Bône, C. Geffroy, G. Fuller, N. Pantoustier, P. Perrin, C. Monteux, Interplay of hydrogen bonding and hydrophobic
356 interactions to control the mechanical properties of polymer multilayers at the oil–water interface, *ACS Macro Letters* 4 (1) (2015) 25–29.
- 357 [20] J. Dupré de Baubigny, P. Perrin, N. Pantoustier, T. Salez, M. Reyssat, C. Monteux, Growth mechanism of polymer membranes obtained by
358 h-bonding across immiscible liquid interfaces, *ACS Macro Letters* 10 (2) (2021) 204–209.
- 359 [21] S. Mun, E. A. Decker, D. J. McClements, Effect of molecular weight and degree of deacetylation of chitosan on the formation of oil-in-water
360 emulsions stabilized by surfactant–chitosan membranes, *Journal of colloid and interface science* 296 (2) (2006) 581–590.
- 361 [22] P. Thanasukarn, R. Pongsawatmanit, D. J. McClements, Utilization of layer-by-layer interfacial deposition technique to improve freeze–thaw
362 stability of oil-in-water emulsions, *Food research international* 39 (6) (2006) 721–729.
- 363 [23] D. Z. Gunes, M. Pouzot, M. Rouvet, S. Ulrich, R. Mezzenga, Tuneable thickness barriers for composite o/w and w/o capsules, films, and their
364 decoration with particles, *Soft Matter* 7 (19) (2011) 9206–9215.
- 365 [24] T. Kuroiwa, Y. Kawauchi, R. Moriyoshi, H. Shino, T. Suzuki, S. Ichikawa, I. Kobayashi, K. Uemura, A. Kanazawa, Biocompatible ho-
366 mogeneous particle formation via the self-complexation of chitosan with oleic acid and its application as an encapsulation material for a
367 water-insoluble compound, *Colloids and Surfaces A: Physicochemical and Engineering Aspects* 624 (2021) 126808.
- 368 [25] K. Xie, C. de Loubens, F. Dubreuil, D. Z. Gunes, M. Jaeger, M. Leonetti, Interfacial rheological properties of self-assembling biopolymer
369 microcapsules, *Soft matter* 13 (36) (2017) 6208–6217.
- 370 [26] M. Maleki, C. de Loubens, K. Xie, E. Talansier, H. Bodiguel, M. Leonetti, Membrane emulsification for the production of suspensions of
371 uniform microcapsules with tunable mechanical properties, *Chemical Engineering Science* 237 (2021) 116567.
- 372 [27] M. M. Mady, M. M. Darwish, S. Khalil, W. M. Khalil, Biophysical studies on chitosan-coated liposomes, *European Biophysics Journal* 38 (8)
373 (2009) 1127–1133.
- 374 [28] L. Chiappisi, M. Gradzielski, Co-assembly in chitosan–surfactant mixtures: thermodynamics, structures, interfacial properties and applica-
375 tions, *Advances in colloid and interface science* 220 (2015) 92–107.
- 376 [29] M. Rinaudo, Chitin and chitosan: Properties and applications, *Progress in polymer science* 31 (7) (2006) 603–632.
- 377 [30] O. Mertins, R. Dimova, Insights on the interactions of chitosan with phospholipid vesicles. part i: Effect of polymer deprotonation, *Langmuir*
378 29 (47) (2013) 14545–14551.
- 379 [31] O. Mertins, R. Dimova, Insights on the interactions of chitosan with phospholipid vesicles. part ii: Membrane stiffening and pore formation,
380 *Langmuir* 29 (47) (2013) 14552–14559.
- 381 [32] M. D. Biviano, L. J. Böni, J. D. Berry, P. Fischer, R. R. Dagastine, Viscoelastic characterization of the crosslinking of β -lactoglobulin on
382 emulsion drops via microcapsule compression and interfacial dilational and shear rheology, *Journal of Colloid and Interface Science* 583
383 (2021) 404–413.
- 384 [33] V. Babak, E. Merkovich, J. Desbrieres, M. Rinaudo, Formation of an ordered nanostructure in surfactant-polyelectrolyte complexes formed
385 by interfacial diffusion, *Polymer Bulletin* 45 (1) (2000) 77–81.
- 386 [34] D. Renggli, A. Aliche, R. H. Ewoldt, J. Vermant, Operating windows for oscillatory interfacial shear rheology, *Journal of Rheology* 64 (1)
387 (2020) 141–160.
- 388 [35] P. Erni, P. Fischer, E. J. Windhab, V. Kusnezov, H. Stettin, J. Läger, Stress- and strain-controlled measurements of interfacial shear viscosity
389 and viscoelasticity at liquid/liquid and gas/liquid interfaces, *Review of Scientific Instruments* 74 (11) (2003) 4916–4924. arXiv:<https://doi.org/10.1063/1.1614433>,
390 [doi:10.1063/1.1614433](https://doi.org/10.1063/1.1614433), [doi:10.1063/1.1614433](https://doi.org/10.1063/1.1614433).
391 URL <https://doi.org/10.1063/1.1614433>
- 392 [36] N. Ali, Rhéospeckle : un nouvel outil d'étude du comportement multi-échelle des matériaux hétérogènes, Ph.D. thesis, Université Grenoble
393 Alpes, thèse de doctorat dirigée par Roux, Denis et Caton, François (2016).
394 URL <http://www.theses.fr/2016GREAI013>
- 395 [37] L. Cipelletti, H. Bissig, V. Trappe, P. Ballesta, S. Mazoyer, Time-resolved correlation: a new tool for studying temporally heterogeneous
396 dynamics, *Journal of Physics: Condensed Matter* 15 (1) (2002) S257.
- 397 [38] H. Bissig, S. Romer, L. Cipelletti, V. Trappe, P. Schurtenberger, Intermittent dynamics and hyper-aging in dense colloidal gels, *PhysChem-*
398 *Comm* 6 (5) (2003) 21–23.
- 399 [39] A. Duri, H. Bissig, V. Trappe, L. Cipelletti, Time-resolved-correlation measurements of temporally heterogeneous dynamics, *Phys. Rev. E* 72
400 (2005) 051401. [doi:10.1103/PhysRevE.72.051401](https://doi.org/10.1103/PhysRevE.72.051401).
401 URL <https://link.aps.org/doi/10.1103/PhysRevE.72.051401>
- 402 [40] S. Barman, G. F. Christopher, Role of capillarity and microstructure on interfacial viscoelasticity of particle laden interfaces, *Journal of*
403 *Rheology* 60 (1) (2016) 35–45.

- 404 [41] W. de Carvalho, M. Djabourov, Physical gelation under shear for gelatin gels, *Rheologica Acta* 36 (6) (1997) 591–609.
- 405 [42] E. Secchi, T. Roversi, S. Buzzaccaro, L. Piazza, R. Piazza, Biopolymer gels with “physical” cross-links: gelation kinetics, aging, heterogeneous
- 406 dynamics, and macroscopic mechanical properties, *Soft Matter* 9 (15) (2013) 3931–3944.

Structural characterization of the interfacial self-assembly of chitosan with
oppositely charged surfactant

Supplementary informations

by R Chachanidze *et al.*

I. INTERFACIAL RHEOMETRY

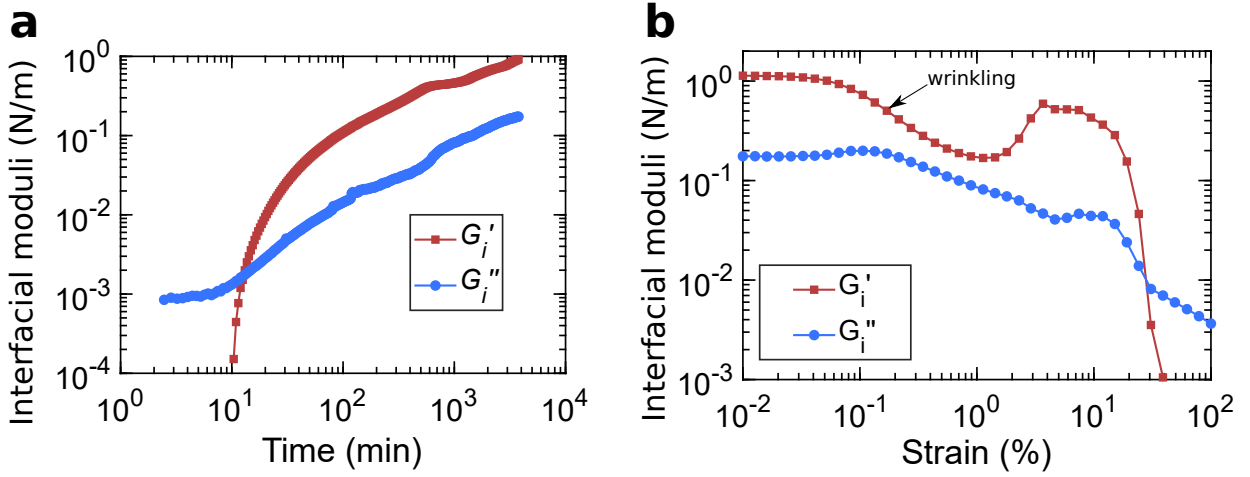


Figure 1: **a:** We performed a long term membrane formation for a single case (0.1% w/w chitosan, 0.1% w/w PFacid , $f = 0.5$ Hz, $\gamma = 0.03\%$) in order to perform a strain sweep on a thick membrane and define the limits of linear elastic regime. **B:** We observed that for long term formed membranes (>24 hours) the linear elastic regime was limited to surprisingly low values of strain ($<0.1\%$). The direct microscopic observation of the membrane decorated with tracing particles during the strain sweep experiments showed that this highly non-linear behaviour was caused by wrinkling instability of the membrane. The deformation of $\approx 20\%$ lead to the rapid decline in G'_i . The direct observation showed that it was caused by the loss of connectivity between the membrane and the bicone.

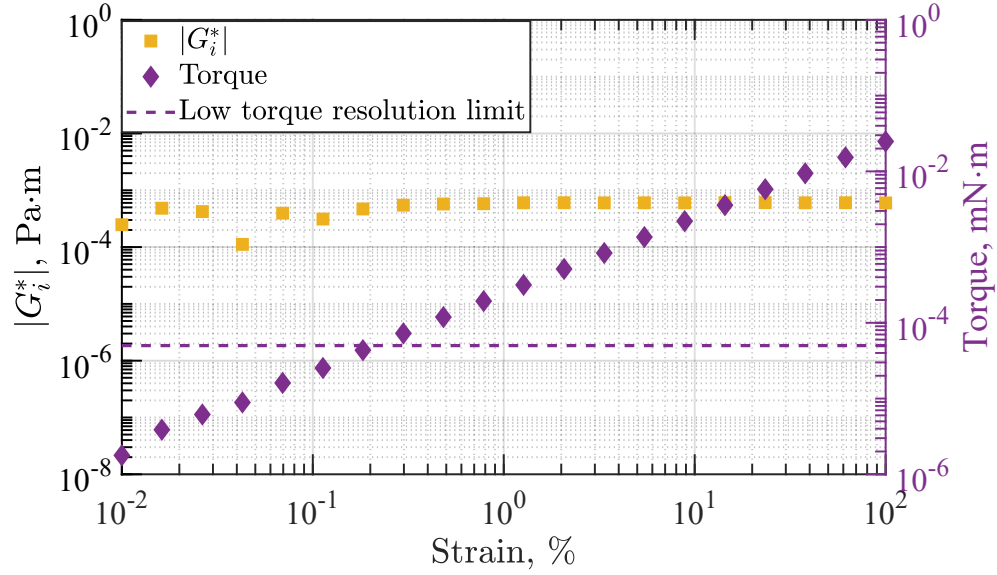


Figure 2: Strain sweep of the chitosan/oil interface. The test was performed with the bicone geometry ($f = 0.5$ Hz). The aqueous phase contained 0.1% w/w chitosan. PFacid was not added to the oil phase. The result illustrates the steady state chitosan/oil interface without the complexation. **Note:** while the stable values of interfacial viscoelastic modulus G_i^* are obtained, without the solid membrane forming at the interface the Boussinesq number is very low ($Bo=0.242$ in this case). Thus this result is qualitative and served as a reference line.

II. DYNAMIC LIGHT SCATTERING

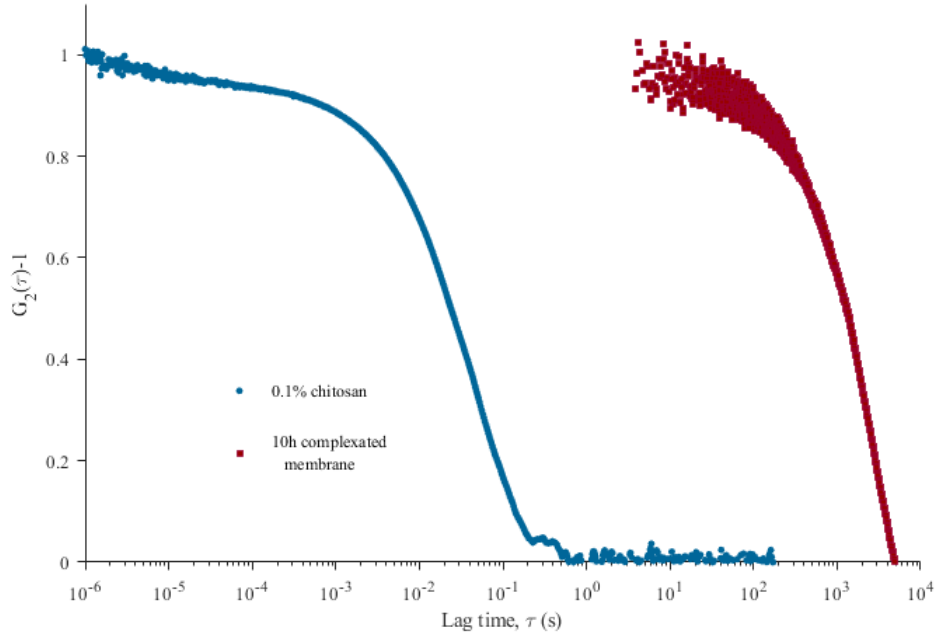


Figure 3: Two distinct cases demonstrating the changes in chitosan/PFAcid membrane DLS signature. The average characteristic relaxation time of chitosan solution (0.1% w/w) was $\tau = 0.88$ s. The relaxation time of fully formed membrane after 10 hours of complexation was 3488.4 s. Note, that DLS signature of the chitosan solution, being a fast process, was acquired using the PM as a receiver, while the DLS signature of the membrane was acquired with fast camera.

III. MEMBRANE THICKNESS MEASUREMENT

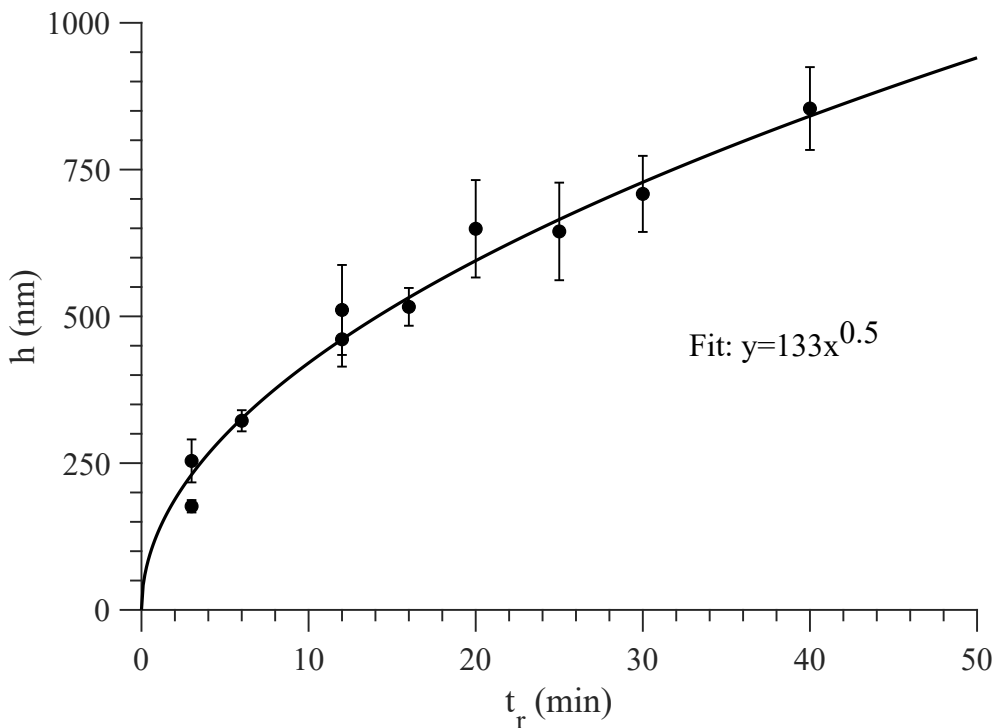


Figure 4: Growth of chitosan/PFacid membrane thickness as a function of reaction time. The square root fitting is consistent with the diffusion driven process. The membranes were grown on a surface of water droplets in oil phase containing chitosan and PFacid respectively as described in the section. The membrane thickness is estimated by measuring the height of the collapsed flat regions on the encapsulated droplets. For SEM, the capsules were dried on a glass with a conductive coating (ITOSOL12 from Solems France). SEM imaging are carried out to image the cross section of membrane using a GeminiSEM 500 (ZEISS) at high vacuum condition. A layer of carbon powder is sprayed on the region of interest and then milled by a focused ion beam (ZEISS NVISION 40). The thickness of the membrane in the dry state is corrected from the measurement of the mass loss during the drying process to calculate the thickness in the wet state. The interfacial membrane was formed via complexation between 3.3% of PFacid and 0.3% chitosan. The error bars are standard deviation.